

High-Sensitivity Radiometry of Air–Water Interface Fast Temperature and Heat Flux Variances

Konstantin P. Gaikovich

Abstract—Fast variances of temperature profile and heat flux through the water–air interface caused by atmospheric turbulence in weak wind conditions have been determined on the basis of measurements of radio brightness evolution of water at the frequencies of 60 and 131 GHz. Two components of the heat flux related to evaporation and to thermal conductivity have been obtained, which enabled us to determine evaporation rate and viscous sublayer depth variances. Statistical parameters of water surface temperature variations have been calculated.

Index Terms—Author, please supply your own keywords or send a blank e-mail to keywords@ieee.org to receive a list of suggested keywords.

I. INTRODUCTION

THIS PAPER continues our investigations [1]–[11] of subsurface radiometry. The theory of radio-emission in a medium (half-space) based on simultaneous solution of emission transfer and thermal conductivity equations has been developed in [1]–[3]. Expressions for brightness temperature of radio-emission as integrals of boundary conditions evolution have been obtained [1], [2] and, next, the inversion of these expressions gave the formulas for the boundary conditions and the temperature distribution (profile) of a medium as integrals of brightness temperature evolution [3]. That enabled us to obtain an exact solution of the problem of one-wavelength temperature profile retrieval. These results have been applied for radiometer investigations of the diurnal heat dynamics in soil (by brightness temperature measurements at the wavelengths of 0.8 and 3 cm), and also for investigations of the atmospheric boundary layer (using measurements at the frequency of 60 GHz in the oxygen band center) [3].

In earlier papers, another radiometry method of the temperature profile retrieval was developed. This method is based on inversion of the frequency dependence of radio brightness [4]–[9]. Interesting results in the subsurface sounding have been obtained using this spectral approach. In particular, temperature profiles have been retrieved in water [1], [5], [6], soils [1], [7], [8], and in living tissues [9]. In stationary media, it proved possible to retrieve by frequency dependence of radio brightness the depth distribution of thermal sources [4]. In those works, the Tikhonov method of generalized discrepancy was used for solution of the corresponding ill-posed problems (Fredholm integral equations of the first kind).

The same spectral approach can also be applied, of course, for investigation of the temperature dynamics in media under nonstationary boundary conditions, but the above-mentioned one-wavelength method has very significant advantages. First, it gives a rigorous solution of the inverse problem. Second, it is much simpler in use because of the compactness and better calibration accuracy of one-channel radiometry system that could be comparable with radiometer sensitivity.

Consequently, we employed this method in [10] for analysis of the dynamics of temperature profile and heat flux through the water–air interface in the process of air turbulization in laboratory conditions. An equation to determine a viscous sublayer depth by the retrieved heat flux dynamics has been obtained and applied in the analysis. The retrieval accuracy of the temperature profile (determined by comparison with the direct measured temperature) amounted to 0.07 K [10]. Next, similar investigation has been performed in outdoor measurements using high-sensitivity radiometers. It allowed us to retrieve fast variances of heat flux and temperature in water caused by natural air turbulence [11]. In this paper, results of the subsequent analysis of those data are presented. It is an important step toward application of this radiometry method to real conditions.

Investigation of the water near-surface thermal regime is especially interesting because temperature gradients in a thin subsurface layer and evaporation from the water surface determine heat exchange between the ocean and the atmosphere. This layer, known as a water cold film [12]–[14], has been widely studied using contact and infrared sensors. Radiometric methods have also been applied [15]. Typically, to determine a heat flux, the difference between the surface sea temperature and the “bulk” water temperature is measured. This approach neglects the temperature profile in a film. Low-inertia falling contact sensors [14] allow us to determine the temperature profile in a cold film, but at fixed place and time, and they inevitably disturb the measured medium. Further development of the proposed high-sensitivity radiometry method could give a new possibility for the real-time noninvasive control of the temperature profile in water and heat exchange through the air–water interface.

II. MEASUREMENTS

Measurements of water medium (see the schematic in Fig. 1) have been carried out using the equipment that included a water pool having size $2 \times 1.5 \times 0.2$ m and radiometers at the frequencies of 60 and 131 GHz [both have been elaborated in Space Research Institute (RAS)] and contact temperature pin-transmitters, which can be placed into water at any given depth. Horn

Manuscript received March 15, 2001; revised January 15, 2003. This work was supported by the RFBR au: please spell RFBR under Grant 96-02-16514.

The author is with the Department of Semiconductor Physics, Institute for Physics of Microstructures, Novgorod 603600, Russia.

Digital Object Identifier 10.1109/TGRS.2003.815668

antennas were placed together in nadir direction 1 m above the water surface. Nominal radiometers sensitivity was 0.01 K at the integration time $\tau = 1$ s. The antenna beam widths were 5° , since the beam footprint on the water had the diameter of about 10 cm. The same water medium at two known different values of temperature is used in the calibration method. The homogeneity and invariability of radio brightness background, its closeness to measured values of brightness temperature (T_b), and the absence of direct solar irradiation were provided by measurements under a plane metal screen (it was somewhat larger in size than the water pool and was placed 10 cm above the antennas). This method [1], [4]–[8] compensates almost completely the surface reflection influence. If the power reflection coefficient of the water is R and the brightness temperature of upwelling radiation of water is $(1 - R)T_b$, the received emission after multiple reflections will be $[(1 - R)T_b + R(1 - R)T_b + R^2(1 - R)T_b + \dots] = T_b$. Actually, two to three reflections are sufficient to achieve needed accuracy of measurements. So, this calibration method, in which the reference brightness temperatures (averaged over the time of 1 min) are assumed to be equal to the corresponding values of water temperatures, provides the condition as if the reflection coefficient were zero. It made possible to achieve the measurement accuracy comparable with the radiometer sensitivity. There remain only small variations of the received brightness temperature because of limited sizes of the “water surface-metal screen” system (part of variances of the atmospheric background radio-emission reflected several times at the screen and at the water). It is an additional noise of about 0.03 K that limits achievable measurement accuracy.

The skin-depth of thermal radio-emission formation $d_{\text{eff}} = 1/\gamma$ (γ is the power absorption coefficient of radio-emission) at the frequency $f = 60$ GHz amounts to $d_{\text{eff}} \cong 0.2$ mm, and at $f = 131$ GHz it is about 0.1 mm. At large values of temperature gradients in the water thermal films, the difference between the surface temperature and the brightness temperature amounts to 0.3 K at $f = 60$ GHz. Such values should be considered as significant for the realized measurement accuracy; they contain important information about processes and should be taken into account in the analysis on the basis of the above-mentioned theory. Measurements at $f = 60$ GHz are more suitable for our goals because this wavelength is in the center of a strong oxygen absorption band where the atmospheric brightness temperature is close to the temperature of the surrounding air. Atmospheric radio brightness variations are comparable with the air temperature variations. Variations of the atmospheric radio brightness at the second wavelength can be much larger and depend on the presence of cloudiness. So, measurements at $f = 131$ GHz were used mainly for comparison. All measurements were carried out under cloudless conditions.

Initial homogeneous temperature distribution in water was obtained by means of mixing and this distribution was unchanged in the absence of air turbulence during a few minutes interval.

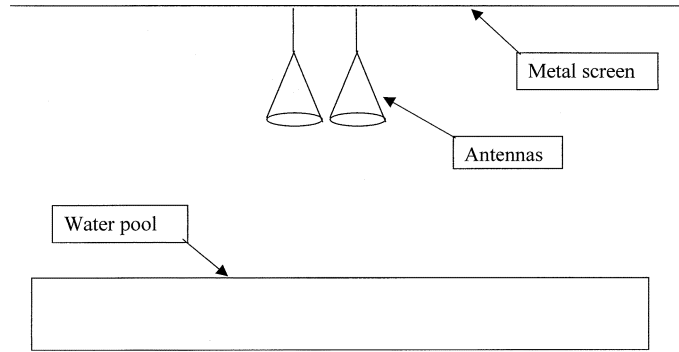


Fig. 1. Scheme of measurements.

III. DETERMINATION OF THE HEAT EXCHANGE THROUGH THE AIR–WATER INTERFACE CAUSED BY AIR TURBULENCE

The main goal of these measurements was to test the ability of high-sensitivity radiometry of retrieving fast variations of temperature and heat flux in the most simple and specific conditions (weak wind, no water convection, or turbulence). It is the next step after laboratory testing [10] to further applications of this method, particularly, in sea conditions.

From the beginning, the water was in the near-stationary condition as a result of sun heating, thermal emission, evaporation, and thermal conductivity balance. Then, by mixing (under a polyethylene film), a homogeneous temperature distribution was achieved, the sun emission was screened, and (after removing the polyethylene film) the water temperature dynamics related to evaporation and thermal exchange due to air turbulence was recorded by radiometers.

The depth of the viscous sublayer above the water surface depends primarily on wind speed variations. Here we suppose that molecular diffusivity in the viscous sublayer is the only process of heat and mass transfer. Above the viscous sublayer there is a region of turbulence. Because the eddy diffusivity coefficient is several orders higher than the molecular diffusivity coefficient, we can assume that all the temperature and water vapor concentration changes occur within this layer. So, we have a two-layer atmosphere model.

It should be mentioned that there are some small variations of water temperature and heat flux, which we are unable to measure because of integration over footprint and time. They are related to high-frequency (small-scale) variations of air turbulence that lead to high-frequency (but small) variations of viscous sublayer depth and, hence, to small variations of water surface temperature. These variations are still smaller because of water thermal inertia smoothing.

The temperature and vapor concentration gradients in the viscous sublayer are inversely proportional to its depth, so variations of these gradients will be strong. The following analysis gives the retrieval of all the details of heat and mass exchange in the air–water system.

The measured evolution $T_B(\tau)$ in the time interval $-\infty < \tau \leq t$ has been used to determine the subsurface temperature profile $T(z, t)$ using the known solution of the system of equations for emission transfer and thermal conductivity equations

[3] for homogeneous half-space $z \leq 0$ (z is depth) with temperature diffusivity coefficient a^2 and radio-emission absorption coefficient γ

$$T(z, t) = \int_{-\infty}^t T_b(\tau)(-z)e^{-(z^2/4a^2(t-\tau))} \frac{d\tau}{\sqrt{4\pi a^2(t-\tau)^3}} + \frac{1}{\gamma a} \int_{-\infty}^t T_b'(\tau)e^{-(z^2/4a^2(t-\tau))} \frac{d\tau}{\sqrt{\pi(t-\tau)}} \quad (1)$$

the second term of which can be integrated by parts for the region $z < 0$

$$T(z, t) = \int_{-\infty}^t T_b(\tau)e^{-(z^2/4a^2(t-\tau))} \cdot \left[\frac{1}{\gamma} \left(\frac{z^2}{2a^2(t-\tau)} - 1 \right) - z \right] \frac{d\tau}{\sqrt{4\pi a^2(t-\tau)^3}} \quad (2)$$

and for the surface temperature $T_0(t) = T(0, t)$, at $z = 0$, where (2) is not valid, (1) transforms into

$$T_0(t) = T_b(t) + \frac{1}{\gamma a} \int_{-\infty}^t T_b'(\tau) \frac{d\tau}{\sqrt{\pi(t-\tau)}} = T_b(t) + \frac{1}{2\gamma a} \int_{-\infty}^t (T_b(t) - T_b(\tau)) \frac{d\tau}{\sqrt{\pi(t-\tau)^3}}. \quad (3)$$

The heat flux through the air-water interface is determined by the time derivative $T_b'(t)$ [3]

$$J(t) = -\frac{k}{a^2\gamma} \left(T_b'(t) + \gamma a \int_{-\infty}^t T_b'(\tau) \frac{d\tau}{\sqrt{\pi(t-\tau)}} \right) \quad (4)$$

where k is the thermal conductivity coefficient. In our case, the integration in (2)–(4) starts from the initially homogeneous temperature distribution $T(z, \tau_{in}) = T_{in}$ ($T_b(\tau_{in}) = T_{in}$) and if we use in the linear equations (2)–(4) the difference $\Delta T_b(\tau) = T_b(\tau) - T_b(\tau_{in})$ to obtain $\Delta T(z, \tau) = T(z, \tau) - T_{in}$, then the lower limit ($-\infty$) in (2)–(4) can be changed to τ_{min} .

This approach is valid if the thermal conductivity is the only process of heat transfer in water. In our previous paper [10], we observed in laboratory conditions the process of convection in water and studied its influence on radiometer measurements and on results of retrieval as well as the influence of water turbulence. We showed the possibility to predict the beginning of convection on the basis of Rayleigh number calculation by retrieved temperature profile. In this paper, as a first step to real conditions, measurements have been carried out in weak wind conditions, when temperature gradients in water are too small to develop convection, so the above expressions are undoubtedly valid.

In the upper (atmospheric) half-space of the air-water interface, the total heat flux determined from (4) can be considered as a sum of different components. Among these components, the latent (related to evaporation) flux is clearly dominant. There is also a thermal conductivity component. It is difficult to calculate the radiation flux component exactly because of the uncertainty of the backward radiation, but the estimation shows that it does not exceed 1% to 3% of the total flux at the maximum. The component related to a horizontal heat flux is also small (not more than 0.5% of the total flux). These two components can be sig-

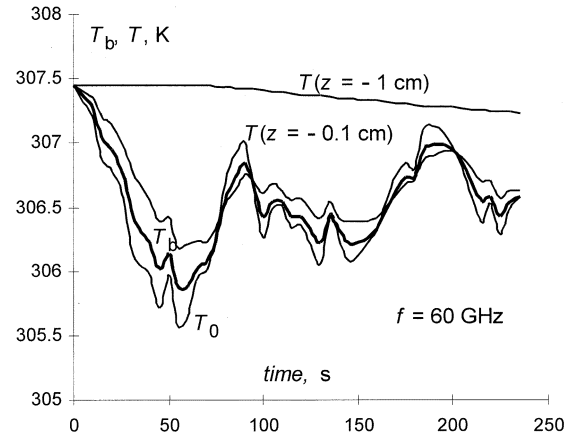


Fig. 2. Radio brightness dynamics $T_b(t)$ related to atmospheric air turbulence (bold line) at frequency 60 GHz and retrieved (by radio brightness T_b at 60 GHz) dynamics of surface temperature $T_0(t)$ and temperature $T(t)$ at depth levels $z = -0.1$ cm and $z = -1$ cm.

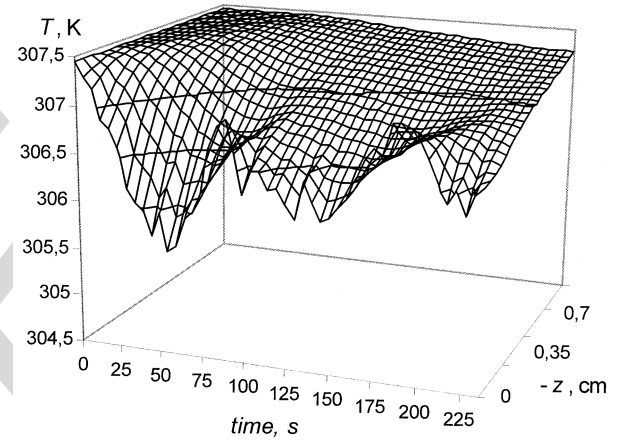


Fig. 3. Retrieved temperature evolution in water related to air turbulence.

nificant only during wind drops, when evaporation diminishes drastically. These components are also independent of the depth of a viscous sublayer and can be considered as additive errors of the total flux that is a sum of two first components.

In the framework of the above-mentioned model, the heat flux $J(t) = -k(dT/dz)(0, t)$ is the sum of the first component related to evaporation and the second one related to molecular temperature conductivity in a viscous sublayer

$$\begin{aligned} J(t) &= J_q(t) + J_T(t) \\ &= -L\rho D_q \frac{dq}{dz}(0) - k \frac{dT}{dz}(0) \\ &= -L\rho D_q \frac{q_a - q(0)}{d} - \rho c_p a^2 \frac{T_a - T(0)}{d} \end{aligned} \quad (5)$$

where q is water vapor concentration, L is specific heat of evaporation, ρ is air density, D_q is vapor diffusivity coefficient, c_p is specific heat capacity at constant pressure, d is viscous sublayer depth, and q_a and T_a are values of vapor concentration and temperature at the turbulent-nonturbulent interface, respectively. The air density is $\rho = (1/R_a)(P/T)$, where P is air pressure and R_a is gaseous constant of air. It was found that typical relaxation time to linear profiles of temperature and vapor concentration in a viscous sublayer is about 0.2 s; hence, it is rea-

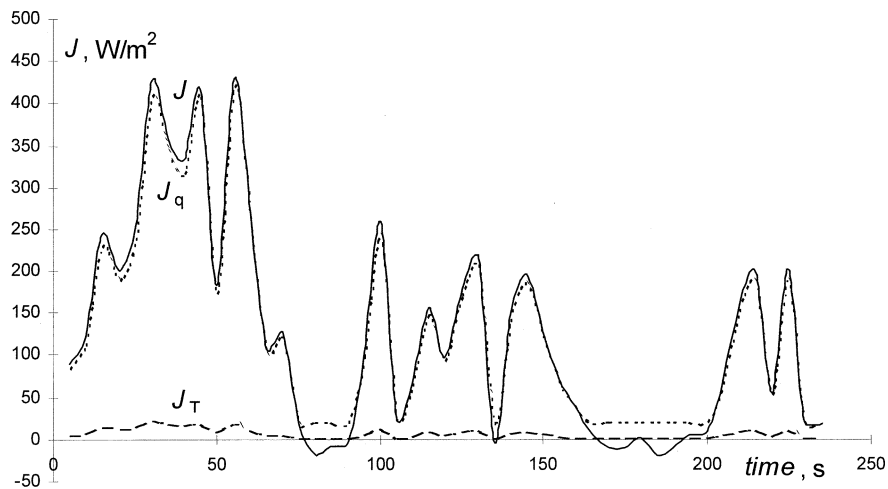


Fig. 4. Dynamics of the heat flux $J(t)$, its evaporation component $J_q(t)$, and its thermal conductivity component $J_T(t)$.

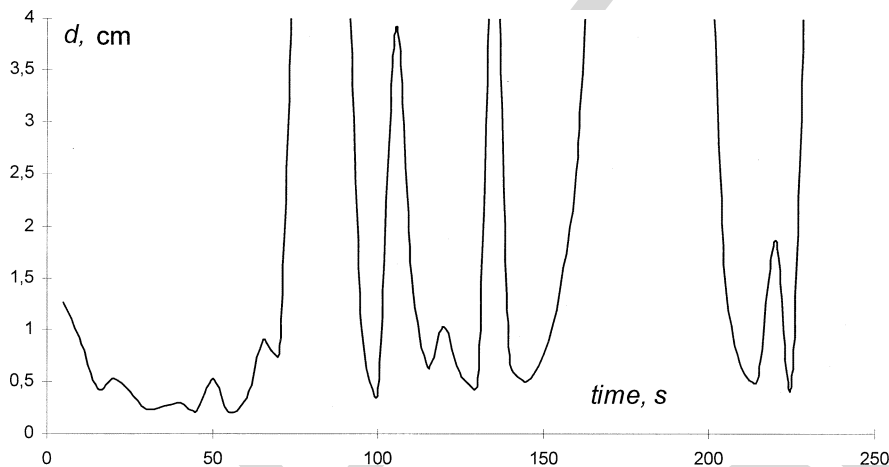


Fig. 5. Retrieved dynamics of the atmospheric viscous sublayer depth.

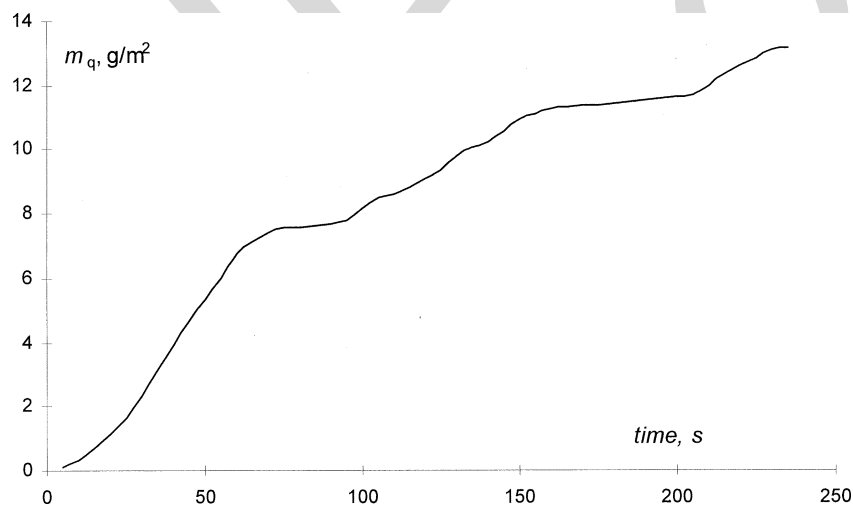


Fig. 6. Retrieved evaporation dynamics.

sonable to suppose that the temperature and concentration gradients are constant. The water vapor concentration at the water surface $q(0)$ can be expressed through saturated concentration that depends on the surface temperature only (see [10]). Hence, all the parameters in (5) depend on water surface temperature

only, and, as it was shown in [10], the expression (5) can be solved as a quadratic equation relative to the viscous sublayer depth d . Both the solutions are physically meaningful, but only the first solution (with plus at the square root) is achieved in the atmospheric turbulence conditions.

The radio brightness variances caused by atmospheric air turbulence variations (after mixing of water) at the frequency of 60 GHz as well as the retrieved evolution of surface temperature, and the temperature at two other depth levels are shown in Fig. 2.

The retrieved temperature variances can be seen in detail in Fig. 3.

It was sunny weather with low wind during the measurements. For the case shown in Figs. 2 and 3, the wind speed was the following: almost steady wind 5–6 m/s in the time interval 0–50 s; dropped to zero in the interval 50–90 s; very light wind 0–3 m/s in 90–160 s; dropped to zero in 160–190; 5–7 m/s in 190–200 s; light wind 3 m/s 200–250 s.

In Figs. 2 and 3, one can see how sharp surface temperature variances transfer to deeper layers of water with more and more delay, where these variances gradually become smooth. The corresponding heat flux dynamics through the air–water interface determined from (5) is shown in Fig. 4.

These results prove that the heat flux has fast and strong variations. It is possible to determine a viscous sublayer depth from (5) and then two components of heat flux related to evaporation and thermal conductivity. These components are also shown in Fig. 4, and variances of the viscous sublayer depth retrieved from (5) are given in Fig. 5. The influence of the evaporation component of the heat flux is obviously predominant. It should be mentioned that small negative values of the total heat flux during the wind drops are unexplained because both its components are positive (the water was warmer than the air). It is possible to see that in time intervals when the wind drops, the depth of a viscous sublayer enhances drastically. It is so large that in this case it is necessary to take into account the inertia of diffusivity in this layer, and the expression (5) is not quite correct. The radiation component can also be responsible for these small negative values (the influence of the horizontal heat flux is also positive).

The viscous sublayer depth was, upon the whole, larger than in the conditions of laboratory measurements [10] where it was about 2 mm. The values above 4 cm are not shown in Fig. 5 because during the wind drops the concept of viscous sublayer itself is inapplicable as well as (5).

It is easy to obtain the evaporation dynamics as integral of the evaporation component

$$m_q(t) = 1/L \int_0^t J_q(t') dt'. \quad (6)$$

The corresponding results are shown in Fig. 6.

IV. COMPARISON OF RESULTS AT TWO WAVELENGTHS

Measurements at $f = 131$ GHz have been carried out mainly for comparison with results at $f = 60$ GHz. The radio brightness dynamics at 60 and 131 GHz for a shorter time period as well as the retrieval dynamics of the surface temperature and the temperature at the depth $z = -1$ mm are given in Fig. 7.

One can see that the difference of retrieved temperatures at $z = -1$ mm agrees well with the rms error of retrieval (0.07 K) obtained in [10]. The retrieval error for the surface temperature was not determined in this paper because of both experimental and theoretical difficulties of this problem. So, data presented

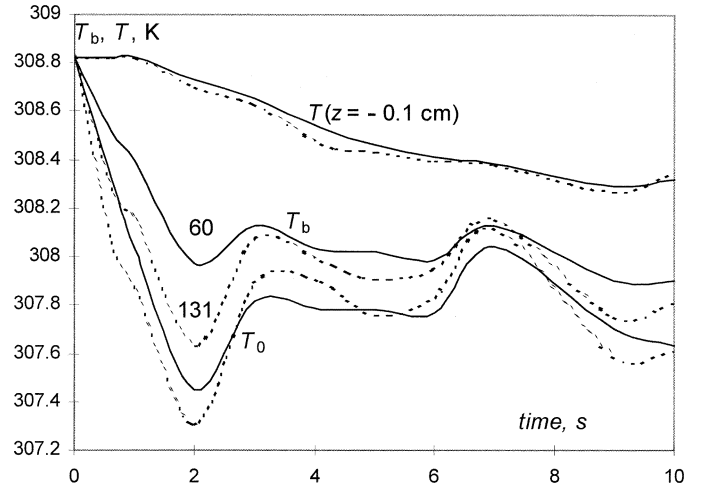


Fig. 7. Radio brightness dynamics $T_b(t)$ at two wavelengths [(solid line) $f = 60$ GHz]; (dashed line) $f = 131$ GHz] and retrieved temperatures T_0 and $T(z = -1$ mm) [(solid line) by T_b at 60 GHz; (dashed line) by T_b at 131 GHz].

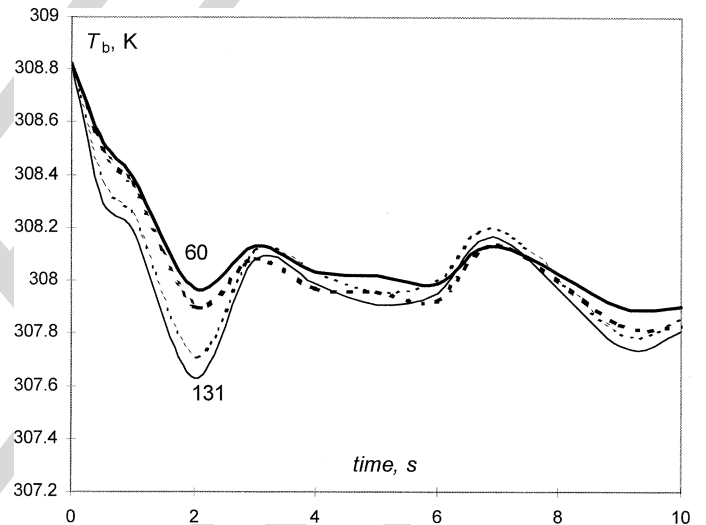


Fig. 8. Radio brightness dynamics at (bold) 60 GHz and 131 GHz and (dashed line) results of their mutual retrieval using (7).

in Fig. 7 give reasonable estimation of this error, which amount to 0.1–0.2 K.

Two-wavelength measurements are also interesting from another point of view. The point is that a formula was obtained in [16] that relates the dynamics of brightness temperatures $T_{b1}(t)$ and $T_{b2}(t)$ at two different frequencies f_1 and f_2

$$T_{b2}(t) = \frac{\gamma_2}{\gamma_1} T_{b1}(t) + \int_{-\infty}^t T_{b1}(\tau) \left(1 - \frac{\gamma_2}{\gamma_1}\right) \gamma_2 a \cdot \left[\frac{1}{\sqrt{\pi(t-\tau)}} - \gamma_2 a e^{(\gamma_2 a)^2 (t-\tau)} \operatorname{erfc}(\gamma_2 a \sqrt{t-\tau}) \right] d\tau \quad (7)$$

where γ_1 and γ_2 are radio-emission absorption coefficients at two different frequencies. The radio brightness dynamics at 60 and 131 GHz and results of retrieval of each of them by the other using (7) are given in Fig. 8. One can see that results of the retrieval of radio brightness dynamics at 60 GHz by data at 131 GHz and vice versa are in a good agreement.

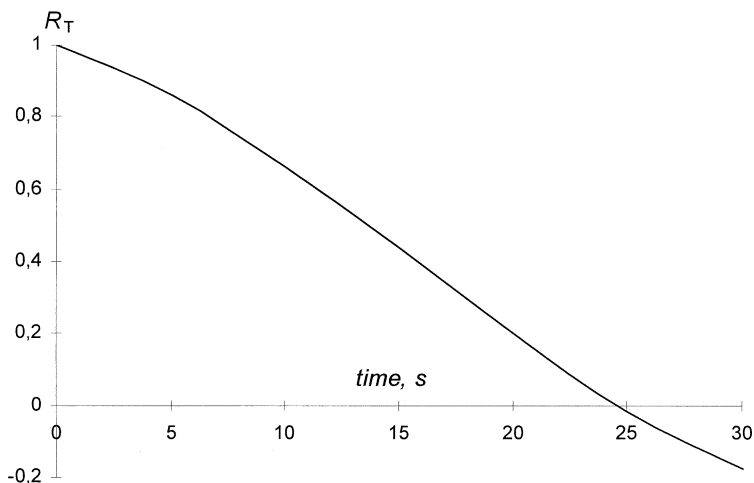


Fig. 9. Autocorrelation coefficient of surface temperature of water.

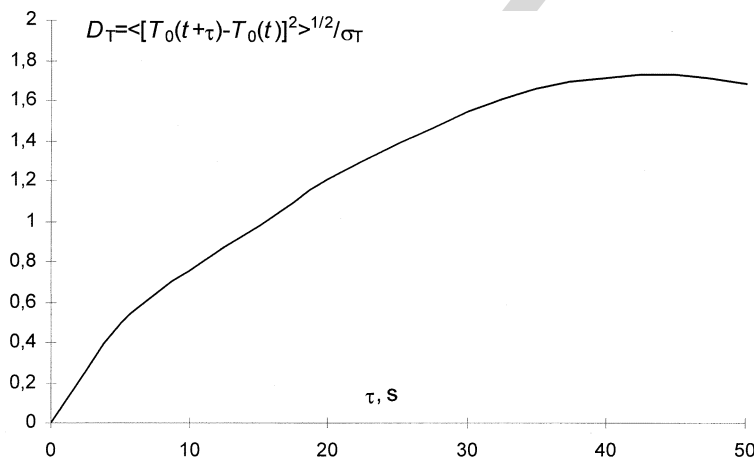


Fig. 10. Normalized structure function of variances of water surface temperature.

V. STATISTICAL ANALYSIS OF VARIATIONS OF WATER SURFACE TEMPERATURE

Results of the retrieval allow for investigation of statistical properties of water temperature variations. Autocorrelation coefficient of water surface temperature $R_T(\tau)$ is shown in Fig. 9. Of course, it is significant for the given weather conditions only. For nonstationary atmospheric processes related to wind speed variances, correlation functions have very limited applicability. In this case, structure functions have much more physical sense. In Fig. 10, one can see the ratio of the square root of the structure function of water surface temperature to its rms variations $\sigma_T = 0.44$ K. If we use Taylor's model of "frozen turbulence," the temporal correlation and structure functions in Figs. 9 and 10 can be considered as the corresponding spatial functions with argument $\rho = V\tau$, where V is the mean wind speed in the near-surface layer. The typical correlation time in Fig. 9 corresponds to the time of transfer of the outer eddy scale in the atmospheric boundary layer (about 100 m) with the wind speed of 5 m/s.

The results show that the rms difference of temperature grows with an increase in the time shift. For $\tau > 25$ s, it becomes greater than 1 K, which exceeds the level of the air temperature variations that have been about 0.05 K at the same time shift

during measurements (determined by variations of the atmosphere radio brightness variations measured at $f = 60$ GHz). This occurs because the influence of evaporation variances is much greater than the thermal exchange between the air and the water due to thermal conductivity.

Note that the typical correlation time of the surface temperature of water is comparable with the time of the cold thermal film formation in turbulent water (about 10 s) that was determined in [10]. So, we can conclude that in the presence of turbulence (a very common case in real conditions) a cold thermal film will experience very rapid and strong depth variations. They will lead to corresponding spatial variations of the film depth. The amplitude of variations depends on air humidity and air-water temperature drop. For example, they will decrease if the air humidity is close to its saturated value and if the air temperature is near the water temperature.

VI. CONCLUSION

The first physical information about fast processes of heat and mass exchange through the air-water interface has been obtained by thermal emission dynamics in natural conditions using high-sensitivity radiometry. Water temperature variances in a

near-surface water layer caused by atmospheric air turbulence have been retrieved in weak wind conditions. Fast evolution of a heat flux through the air-water interface has been revealed. A viscous sublayer depth in the air has also been found, and shown to have strong variations. It plays a regulating role in the thermal exchange process because heat and mass fluxes are inversely proportional to this depth. Statistical parameters of the surface temperature of water have been found, and it has been revealed that variations of the surface temperature in the conditions of experiment are an order of magnitude greater than air temperature variations.

The results show the possibility of the radiometry method application for investigation of fast processes of the heat and mass exchange between the atmosphere and the water surface. It can give valuable information about this process in various weather and climate conditions. Especially interesting would be investigations of a spatial structure of heat exchange process, in particular, of spatial variability of viscous sublayer depth. Sharp variations at the length of tens of meters can be expected that may give a picture of strongly inhomogeneous heat and water vapor fluxes in the atmosphere from the water surface, which influence the process of atmospheric turbulence and convection. The next step in developing of this method is investigation of its potentialities at stronger wind, in the conditions of convection and turbulence of water.

Similar investigations of thermal emission and thermal regime dynamics for various kinds of background may also give interesting results about the atmosphere-background interaction.

ACKNOWLEDGMENT

The author is grateful to R. V. Troitsky [Radiophysical Research Institute (Nizhny Novgorod)] for assistance in measurements.

REFERENCES

- [1] K. P. Gaikovich, A. N. Reznik, and R. V. Troitskii, "Microwave subsurface profile thermometry," in *Dig. IGARSS'91*, vol. 3. Espoo, Finland, 1991, pp. 1195-1198.
- [2] K. P. Gaikovich, "Radiometry of the dynamics of the temperature, thermal flow and Earth's surface parameters using thermal evolution equations," *Sov. J. Remote Sens.*, vol. 8, pp. 1028-1042, 1991.
- [3] K. P. Gaikovich, "Simultaneous solution of emission transfer and thermal conductivity equations in the problems of atmosphere and subsurface radiothermometry," *IEEE Trans. Geosci. Remote Sensing*, vol. 32, pp. 885-889, July 1994.
- [4] K. P. Gaikovich, "Determination of heat sources by thermal radiation of a half-space with steady-state temperature distribution," *Radiophys. Quant. Electron.*, vol. 34, pp. 320-323, 1991.

- [5] K. P. Gaikovich, A. N. Reznik, M. I. Sumin, and R. V. Troitskii, "Determination of the temperature profile of the surface layer of water from its microwave emissions," *Izvestia, Acad. Sci., U.S.S.R., Atmos. Oceanic Phys.*, vol. 23, pp. 569-574, 1987.
- [6] K. P. Gaikovich, A. N. Reznik, and R. V. Troitskii, "Radiometry of dynamics of water-medium temperature by internal-wave transmission," *Radiophys. Quant. Electron.*, vol. 36, pp. 139-143, 1993.
- [7] K. P. Gaikovich and A. N. Reznik, "Retrieval of surface thermal history from radio thermal spectrum," *Radiophys. Quantum Electron.*, vol. 32, pp. 987-993, 1989.
- [8] K. P. Gaikovich, A. N. Reznik, and R. V. Troitskii, "A method to determine the subsoil temperature profile and depth of soil freezing," *Radiophys. Quant. Electron.*, vol. 32, pp. 1082-1088, 1989.
- [9] K. P. Gaikovich, M. I. Sumin, and R. V. Troitskii, "Determination of internal temperature profiles by multifrequency radiothermography in medical applications," *Radiophys. Quant. Electron.*, vol. 31, pp. 786-793, 1988.
- [10] K. P. Gaikovich and R. V. Troitsky, "Dynamics of temperature profile, heat, and mass exchange through air-water interface by measurements of thermal radio emission evolution at 60 GHz," *IEEE Trans. Geosci. Remote Sensing*, vol. 36, pp. 341-344, Jan. 1998.
- [11] K. P. Gaikovich and R. V. Troitsky, "The influence of air-water boundary conditions on thermal radio emission at 2, 5 and 8 mm," in *Proc. 3rd Int. Kharkov Symp. Physics and Engineering of Millimeter and Submillimeter Waves (MSMW'98)*, vol. 2, Kharkov, Ukraine, Sept. 15-17, 1998, pp. 509-511.
- [12] G. G. Khundzhua, A. M. Gusev, Ye. G. Andreev, V. V. Gurov, and N. A. Skorokhvatov, "Structure of the cold surface film of the ocean and heat transfer between the ocean and the atmosphere," *Izvestiya, Atmos. Ocean. Phys.*, vol. 13, pp. 506-509, 1977.
- [13] A. I. Ginzburg, A. G. Zatsepin, and A. N. Fedorov, "Fine structure of the thermal boundary layer in the water near the air-water interface," *Izvestiya, Atmos. Ocean. Phys.*, vol. 13, pp. 876-882, 1977.
- [14] A. V. Soloviev and N. V. Vershinsky, "The vertical structure of the thin surface layer of the ocean under conditions of low wind speed," *Deep-Sea Res.*, vol. 29, pp. 1437-1449, 1982.
- [15] Y. G. Trokhimovski, E. R. Westwater, J. Han, and V. Y. Leusky, "Air and sea surface temperature measurements using a 60-GHz microwave rotating radiometer," *IEEE Trans. Geosci. Remote Sensing*, vol. 36, pp. 3-16, Jan. 1998.
- [16] K. P. Gaikovich, "Stochastic theory of temperature distribution and thermal emission of half-space with random time-dependent surface temperature," *IEEE Trans. Geosci. Remote Sensing*, vol. 34, pp. 582-587, Mar. 1996.

Konstantin P. Gaikovich was born on May 30, 1953, in Nizhny Novgorod, Russia. He graduated from Nizhny Novgorod State University in 1975. He received the Ph.D. and the Dr.Sci. degrees from the Radiophysical Research Institute, Nizhny Novgorod, in 1984 and 1994, respectively, both in physics and mathematics.

He is currently a Leading Research Associate with the Institute for Physics of Microstructures of Russian Academy of Sciences, Nizhny Novgorod. His research interests are physical inverse problems and images reconstruction, including the scanning microscopy (tunneling, near-field optical, atomic-force, and microwave), the subsurface radiometry of dielectric media (water, soils, living tissues), the noninvasive diagnostics of superconductors, and the remote sensing of the atmosphere using passive microwave and refraction measurements. He has written papers in the area of the planet radio astronomy and the gases spectroscopy. He has published more than 200 journal articles and conference papers.